



**ACCEPTED ON ANNALS OF GEOPHYSICS, 62,
2019; Doi: 10.4401/ag-8131**

**Variations of ion density and temperature as
measured by ROCSAT-1 satellite over the Indian
region and comparison with IRI-2016 model**

**Geeta Rana^{1*}, A Bardhan², D K Sharma², M K Yadav¹, Malini
Aggarwal³ and Jyotika Dudeja⁴**

¹Department of Humanities and Applied sciences, YMCA University of Science and Technology, Faridabad-121006 ²Department of Physics, ManavRachna University, Faridabad-121001,

³Indian Institute of Geomagnetism, Navy Nagar, Mumbai-400005

⁴Department of Mathematics, Pt. J.L. N. Govt. college, Faridabad-121002

*Email: geetika72@gmail.com/ jointcoe@mru.edu.in

1 Variations of ion density and temperature as measured by ROCSAT-1 satellite over
2 the Indian region and comparison with IRI-2016 model

3
4 Geeta Rana^{1*}, A Bardhan², D K Sharma², M K Yadav¹, Malini Aggarwal³ and Jyotika Dudeja⁴

5 ¹*Department of Humanities and Applied sciences, YMCA University of Science and Technology, Faridabad-121006*

6 ²*Department of Physics, ManavRachna University, Faridabad-121001,*

7 ³*Indian Institute of Geomagnetism, Navy Nagar, Mumbai-400005*

8 ⁴*Department of Mathematics, Pt. J.L. N. Govt. college, Faridabad-121002*

9 *Email: geetikarana72@gmail.com/ jointcoe@mru.edu.in

10
11 **Abstract** -Topside ionospheric parameters-total ion density (Ni) and ion temperature(Ti) have
12 been analysed at low latitude region with changing solar activity (years 1999 to 2003).The Ni
13 and Ti data collected from ROCSAT-1 satellite has been compared with the estimated values of
14 IRI-2016 model. The annual diurnal features observed for Ni (measured by ROCSAT-1) are: a
15 minimum value just before local sunrise (~04:00/05:00 LT), a day-time peak (~13:00/14:00 LT)
16 and then a gradual decrement throughout the evening and nighttime. The annual diurnal variation
17 of Ti (measured by ROCSAT-1) shows that Ti exhibits a morning peak (morning overshoot,
18 ~07:00 LT), a day-time trough, a secondary peak (evening enhancement) followed by nighttime
19 minima and a minimum value before the sunrise. The distinct annual diurnal feature observed by
20 the IRI model is the presence of a secondary evening peak in Ni which is absent in Ti, which is
21 exactly opposite to the trend measured by ROCSAT-1. Some other discrepancies observed in the
22 model are:overestimation of Ni during all the years, specifically in the morning and evening
23 time; overestimation of Ti, during the entire day except in the morning peak hours of the year
24 1999, 2000 and 2003.For each year, the hourly averaged ROCSAT-1 measured value of Ni and
25 Ti has been correlated with the estimated value of IRI-2016 model. The correlation coefficient
26 factor R^2 is ~ 0.8 for Ni and ~ 0.9 for Ti respectively. The variations of Ni and Ti with changing
27 solar flux have also been studied. The ionospheric parameters are found positively and linearly
28 correlated with solar-flux (F10.7). The correlation coefficient factor R^2 for Ni and Ti with F10.7
29 is ~ 0.8 and ~ 0.9 respectively.

30 **Keywords-** Topside ionosphere, ion density, ion temperature, solar flux, solar activity, IRI
31 model

32 **1. Introduction**

33 The solar radiations are the primary cause of ionization of the Earth's atmosphere. Specifically,
34 the X-ray and extreme ultraviolet radiations are the basic drivers at the base of the plasma
35 density distribution in the ionosphere. It is well known that ionospheric plasma and temperature
36 varies with respect to the latitude, altitude, season, geomagnetic and solar activities [Fejer 1997,
37 and Otsuka et al.1998]. The morphology and dynamics of equatorial and low latitude regions is
38 different compared to the mid and high latitude ones.This is because in the low latitude and
39 equatorial regions there occur some unique phenomenon such as equatorial ionization anomaly
40 (EIA), equatorial electrojet (EEJ), plasma fountain, equatorial spread-F (ESF), equatorial wind
41 and temperature [Bhuyan et al. 2002, Prabhakaran Nayar et al. 2004].The EIA is an important
42 characteristic of low latitude ionosphere, which is basically a trough in plasma density at
43 magnetic equator and two crests at around $\pm 15^\circ$ on both sides of the equator. The theory at the
44 base of EIA was proposed by Martyn[1947], who said that the action of the eastward electric
45 field generated perpendicular to the geomagnetic field linesuplifts ($E \times B$ drift) the plasma to
46 altitudes greater than 800km. The uplifted plasma thereafter diffuses along the geomagnetic field
47 lines to the north and south of the equator under the action of gravity and pressure gradient
48 [Hanson and Moffett 1966, Ren et al. 2008]. Hence, forming the ionization trough at the equator.
49 The prereversal enhancement (PRE) phenomenon is also a significant featureof low latitudes.
50 Near the sunset, the eastward electric field shows a strong enhancement just before reverting to
51 westward. This phenomenon causes a sudden rise in the height of F-layer in the evening.

52 In order to understand the really complex dynamics of low latitude ionosphere, the coupling
53 between the topside ionosphere and protonosphere and all related processes, many researchers
54 have worked to study the variations of low latitude ionospheric parameters [Balan et al. 1997,
55 Bhuyan et al. 2002,Watanabe and Oyama 1996, Zhang and Holt 2004, Liu et al. 2007a]. For
56 example, the electron density and temperature at height of ~ 600 km has been investigated with
57 the help of Hinotori satellite which shows that the electron temperature rises sharply in the
58 morning (known as morning overshoot), declines after that and increases again in the evening
59 (known as evening overshoot) [Watanabe and Oyama 1996]. By utilising Millstone Hill radar

60 data, the daytime increment of electron temperature is found more prominent in summer with
61 increasing solar activity than in winter, while the ion temperature is higher during decreasing
62 solar activity [Zhang and Holt 2004]. Again with the Hinotori satellite measurements in the low
63 latitudes, a strong annual anomaly of plasma density has been observed by Su et al. [1998],
64 Bailey et al. [2000], while an electron density semi-annual anomaly has been observed by using
65 Japanese middle and upper atmosphere (MU) radar [Balan et al.2000]. The features of total ion
66 density in the topside ionosphere (840 km) were also observed through the Defence
67 Meteorological Satellite Program (DMSP) and they have reported an annual asymmetry in the
68 rising and declining phases of solar activity [Liu et al. 2007a].The ion density distribution at low
69 latitudes during solar minimum equinoctial conditions has been simulated by using a time
70 dependent model based on the solution of the plasma continuity equation and the results were
71 compared with the observations made by SROSS-C2 satellite [Bhuyan and Kakoty2001, Bhuyan
72 et al. 2002].The variations in electron and ion temperature and density within a region of $\pm 30^\circ$
73 latitude and 200-1000 km of altitude, have been studied by using the time-dependent three-
74 dimensional simulation technique by Watanabe et al. [1995] and they showed a strong effect of
75 plasma drift in the equatorial F-region. At low latitudes, the variations in plasma temperature
76 under equinoctial conditions for low, medium and high solar activity have been studied by Balan
77 et al. [1997]. They made a comparison between values of plasma temperature, modelled by the
78 Sheffield University Plasmasphere Ionosphere model (SUPIM), and ones measured by the
79 Hinotori satellite and found an anomalous variation in temperature from evening to pre-mid
80 night.The atmospheric neutral winds along with the ionospheric dynamics are considered the
81 dominant factors for perturbing the behaviour of plasma density and temperature [Liu et al.
82 2007b, Rishbeth and Muller-Wodarg 2006, Zou et al. 2000, Mendillo et al. 2005].
83 Previous studies have shown that for low latitudes sufficient theories and observations are
84 available for total electron content TEC and electron density but there is a gap concerning the ion
85 density and the ion temperature. The present study focuses on the variations of total ion density
86 (N_i) and ion temperature (T_i), in the low latitude topside ionosphere, for different solar activities,
87 as recorded by ROCSAT-1between 1999 and 2003; a comparative study with the output of the
88 IRI-2016 model has been also performed. Although the IRI model has been continuously
89 improved [Bilitiza et al. 2017], it still shows some shortcoming at equatorial and low latitude

90 regions. Hence, the present analysis is then an additional contribute for testing and understanding
91 advantages and disadvantages of the IRI model.

92 **2. Data Analysis**

93 The ion density and ion temperature data used in the present study have been taken from the
94 ionospheric plasma electrodynamics instrument (IPEI) onboard ROCSAT-1 satellite. The
95 selected region for the analysis lies between 5-35°Geo.N to 65-95°Geo. E in the altitude range of
96 around 600±50 km.

97 The ROCSAT-1 satellite was launched in 1999 and its mission ended in 2004. It had a circular
98 orbit at an average altitude of around 600 km with an orbit inclination angle of 35°[Su et al.
99 1999, Chang et al. 1999].The instrument IPEI onboard the satellite had four sensors and made
100 measurements for ion density, ion temperature, ion composition and drift velocity. The detailed
101 information about IPEI is given in Yeh et al. [1999 a, b].

102 The IRI-2016 model data has been obtained online from
103 https://ccmc.gsfc.nasa.gov/modelweb/models/iri2016_vitmo.php. It is an empirical model which,
104 for a specified time, date and location, provides monthly average values of electron temperature,
105 ion composition, ion temperature, equatorial vertical ion drift and vertical ionospheric electron
106 content in the ionospheric altitude range of 50-2000 km [Bilitza, 1991, Bilitza et al. 2017,
107 Bilitza, 2000].

108 **3. Results and Discussion**

109 The solar flux index (F10.7) data has been retrieved from the website
110 <https://omniweb.gsfc.nasa.gov/form/dx1.html>. Based upon the strength of yearly solar flux
111 magnitude F10.7, the years (1999-2003) have been categorized as rising, higher and
112 declining phases of solar activity. The year 1999 (F10.7~153.9 sfu),-is considered as a rising
113 phase of solar activity; the year 2000 (F10.7~180 sfu), 2001(F10.7~ 181.1 sfu) and
114 2002(F10.7~179.4 sfu) as high solar activity years; the year 2003(F10.7~128.4 sfu) as the
115 declining phase of solar activity. Figure 1 represents the variation of F10.7 flux during the
116 years 1999-2003(upper panel) and yearly averaged data count from 1999-2003 as measured
117 by ROCSAT-1 satellite (lower panel).

118 *3.1. Annual–Diurnal variation of total ion density, Ni*

119 Figure 2, represents the annual variation of hourly averaged total ion density measured by
120 ROCSAT-1 satellite (red coloured triangles) and estimated by IRI-2016 (black coloured circles),
121 during different solar activity phases. The calculations for the IRI model have been made for
122 each month and thereafter the monthly values were averaged for every year. The diurnal features
123 shown by Ni as measured by ROCSAT-1 satellite during the year 1999-2003 are: a daytime peak;
124 nighttime minima; an absolute minimum just before the local sunrise.

125 During the rising (1999) and declining (2003) phases of solar activity, Ni shows a minimum of
126 $\sim 4.16\text{E}+04$ and $\sim 2.94\text{E}+04$ cm^{-3} respectively during pre-sunrise hours ($\sim 04:00/05:00$ LT).
127 Analysis by using Stretched Rohini Satellite Series (SROSS-C2) data measurements has also
128 shown a minimum density of Ni just before local sunrise [Bardhan et al. 2014]. Thereafter, Ni
129 increases gradually due to photoionization of the neutral particles and attains a maximum value
130 of $5.08\text{E}+05$ to $\sim 3.62\text{E}+05$ cm^{-3} during the day time ($\sim 14:00 /15.00$ LT). Ni then starts decreasing
131 continuously through the evening and nighttime hours.

132 During high solar activity years 2000, 2001 and 2002 the minimum values of Ni observed during
133 pre-sunrise hours ($\sim 04:00/05:00$ LT) are $\sim 6.16\text{E}+04$, $6.66\text{E}+04$ and $6.30\text{E}+04$ cm^{-3} respectively.
134 The peak value of Ni observed in the afternoon hours ($\sim 13.00/14.00$ LT) is $6.96\text{E}+05$, $7.28\text{E}+05$
135 and $8.16\text{E}+05$ cm^{-3} during 2000, 2001 and 2002 respectively.

136 According to the IRI model, the diurnal features shown by Ni are: a daytime relative maximum;
137 a secondary absolute maximum during late evening hours; nighttime minima with an absolute
138 minimum during pre-sunrise hours. During the years 1999 and 2003, Ni shows an absolute
139 minimum of $\sim 6.5\text{E}+04$ cm^{-3} and $\sim 4.39\text{E}+04\text{cm}^{-3}$ respectively at $\sim 05:00$ LT; the daytime peaks as
140 $3.8\text{E}+05$ cm^{-3} and $\sim 2.8\text{E}+05$ cm^{-3} respectively at $\sim 14:00$ LT. The secondary absolute peak during
141 1999 is $3.78\text{E}+05$ cm^{-3} at $\sim 19:00$ LT whereas, in the year 2003 there is no secondary peak, so the
142 daytime maximum becomes the absolute one.

143 During the high solar activity years 2000, 2001 and 2002 the absolute minimum values of Ni
144 observed at $\sim 5:00$ LT is $\sim 9.48\text{E}+04$, $9.13\text{E}+04$ and $8.77\text{E}+04$ cm^{-3} respectively; the day time
145 peaks at $\sim 14:00$ LT is $5.21\text{E}+05$, $4.97\text{E}+05$ and $4.72\text{E}+05$ cm^{-3} respectively; the evening
146 absolute maximum is modelled at $\sim 19:00$ LT as $5.71\text{E}+05$, $5.30\text{E}+05$ and $4.86\text{E}+05$ cm^{-3} . The

147 results of Figure 2 show that during high solar activity years higher day-time peaks of Ni are
148 attained as compared to the rising and declining phases of solar activity. Hence, photoionization
149 can be considered as the primary cause of daytime peaks. Moreover, this figure also shows that
150 during all the investigated years (1999-2003), if compared to measurements made by ROCSAT -
151 1, the IRI model predicts higher values of Ni in the pre-sunrise hours and lower values of Ni
152 during daytime. A further feature is that the IRI model shows evening enhancement that are not
153 been observed by ROCSAT-1.

154 *3.2. Annual –Diurnal variation of ion temperature, T_i*

155 The annual variation of hourly averaged ion temperature measured by ROCSAT-1 (red coloured
156 triangles) and estimated by IRI-2016 (black coloured circles) during different phases of solar
157 activity is represented in Figure 3. The study region for T_i is around 600 km which is not the
158 isothermal region of the ionosphere because the temperature is found to increase in the topside
159 ionosphere [Farley et al. 1967].

160 The diurnal features observed by ROCSAT-1 measurements for T_i during years 1999-2003
161 shows that T_i presents a minimum value during pre-sunrise hours and as the sun progresses, the
162 T_i exhibits a sharp increment known as the morning overshoot [Aggarwal et al. 2007, Sharma et
163 al. 2010]. Owing to photoionization, photoelectrons gain higher energy which they share with the
164 surrounding electrons and ions through coulomb-collision; consequently, because of lesser
165 electron/ion density in early morning hours, ion temperature starts increasing rapidly and attains
166 a maximum/peak value at ~07:00 LT [Balan et al. 1996, Su et al. 1995, Bardhan et al. 2015,
167 Oyama et al. 1996]. After attainment the morning peak, T_i experiences a daytime trough, and
168 then, due to the pre-reversal enhancement phenomenon [Balan et al. 1997], it shows an evening
169 enhancement followed by a nighttime decrease.

170 During the years 1999 and 2003, at ~ 07:00 LT, T_i shows morning peaks of ~1565 K and
171 ~1491K respectively, while secondary peaks present values of ~1348 K and ~1292 K
172 respectively at ~ 17/18:00 LT. During the high solar activity years, 2000, 2001 and 2002, the
173 morning peaks are 1525K, 1504 K and 1457 K (at 07:00 LT), whereas the secondary peaks are
174 ~1400K, 1394 K and 1370K respectively at 16/17:00 LT. The nighttime T_i values are also
175 observed to be higher during high solar activity years (~950 K) as compared to those of rising

176 and declining solar activity years (~850 K). This may be due to the adiabatic expansion and
177 compression of the plasma, flowing across the equator and along the field lines [Hanson et al.
178 1973]. The same nighttime plasma features have been observed with the help of the Orbiting
179 Geophysical Observatory satellite (OGO-6) at an altitude of 500 km [Bailey et al. 1973].

180 According to the IRI model, the diurnal features shown by Ti are typical diurnal ones, with
181 higher values during daytime and lower values during nighttime. For years 1999 and 2003, the
182 morning peaks of Ti are observed as ~1475K and 1449 K respectively at ~ 07:00 LT. For years
183 2000-2002, the morning peaks of Ti are of higher magnitude i.e. ~1500K. The secondary peak of
184 Ti visible in ROCSAT-1 measurements is not represented by IRI-2016 model.

185 The annual-diurnal behaviours of Ni and Ti show a different variation pattern. Specifically,
186 during daytime, when Ti presents a trough, Ni shows a peak value. For the topside ionosphere
187 over India, also Borgohain and Bhuyan [2012] investigated Ni and Ti and they observed a
188 positive correlation between them during high solar activity and a negative correlation during
189 low solar activity.

190 **3.3 Assessment of IRI-2016 model estimations with ROCSAT-1 measurements**

191 *3.3.1 Relative variation of Ni*

192 To perform an analysis of the relative variation of Ni as measured by ROCSAT-1 and calculated
193 by IRI-2016 model, the ratios (Ni_{ROCSAT}/Ni_{IRI}) have been plotted in Figure 4 (upper panels). This
194 figure shows that during the whole investigated period (1999-2003) the IRI model overestimates
195 the Ni measurements by ROCSAT-1 during nighttime and pre-sunrise hours, whereas
196 underestimates them during daytime. Largest differences of ratios are obtained during 12-14:00
197 LT and 22-04:00 LT where values vary from 0.4 (lower side; year 1999) to 1.7 (upper side; year
198 2002). Only during the local time ~09-11:00 and ~17-18:00 LT the ratio is equal to ~1, which
199 means that the Ni value measured by ROCSAT-1 is similar to that modelled by IRI.

200 Anyhow, Figure 2 shows that the diurnal pattern of Ni as measured by ROCSAT-1 and estimated
201 by IRI are similar. With regard to this issue, Figure 4 (lower panels) shows the scatterplots
202 between the two data sets (measured and estimated), along with the corresponding linear fit and

203 the value of the correlation coefficient R^2 . R^2 for 1999 and 2003 is found to be 0.84 and 0.89
204 respectively, while during high solar activity years (2000-2002) is found to vary from 0.73-0.85.

205 *3.3.2 Relative variation of T_i*

206 To perform an analysis of the relative variation of T_i as measured by ROCSAT-1 and measured
207 by IRI-2016 model, the ratios ($T_{iROCSAT}/T_{iIRI}$) have been plotted in Figure 5 (upper panels).

208 From the graphs, it can be seen that during all the years (1999-2003) the ratio values are below 1,
209 which means overestimated values of T_i modelled by the IRI model except during few morning
210 peak hours in years 1999, 2000 and 2003.

211 Figure5 (lower panels) shows scatter plots between modelled and measured data, along with the
212 corresponding linear fit and the value of correlation factor R^2 . R^2 is found to be 0.86 during years
213 1999 and 2003, while, during high solar activity years 2000-2002, is found to vary from 0.87-
214 0.90.

215 *3.4. Relationship of N_i and T_i with Solar flux index ($F_{10.7}$)*

216 The solar flux, $F_{10.7}$ is very often used as an index to monitor the solar activity. Since the solar
217 radio emission takes place from the chromosphere and corona, it indicates variations occurring in
218 the Sun during different phases of solar activity [Tapping 2013]. Figure 6 shows scatter plots of
219 N_i vs $F_{10.7}$ and T_i vs. $F_{10.7}$. To plot this figure, yearly averaged values of $F_{10.7}$, N_i and T_i
220 during the daytime (10:00-16:00 LT) have been utilized. The correlation coefficient R^2 between
221 N_i and $F_{10.7}$ is found to be 0.83 for ROCSAT measured values (Fig 6a) and 0.97 between IRI
222 estimated values and $F_{10.7}$ (Fig 6b). This shows that photoionization via extreme ultraviolet
223 radiation remains a major source of ionization in our selected region of study. This confirms
224 what found by Bardhan et al. [2014] who observed higher photoionization during high solar
225 activity in the year 2000 compared to that of the low solar activity in the year 1995, using
226 SROSS-C2 satellite data.

227 Instead, the correlation coefficient R^2 between T_i and $F_{10.7}$ is found to be 0.97 for ROCSAT
228 measured values (Fig 6c) and 0.94 for IRI estimated values (Fig 6d). Both R^2 values are pretty
229 similar to each other during years 1999-2003, which indicates that T_i data during daytime
230 (10:00-16:00 LT) is in good agreement with the solar flux index.

231 4.Conclusions

232 In the present study, we have examined the variation of topside ionospheric parameters,
233 specifically the total ion density, Ni and the ion temperature, Ti, at low latitudes during different
234 phases of solar activity (1999-2003). The Ni and Ti data has been obtained from ROCSAT-1
235 satellite and then a comparison is made with the estimations of the IRI-2016 model. The findings
236 of the present analysis can be summarized in the following points.

- 237 1. The annual diurnal analysis of Ni (measured by ROCSAT-1) shows a minimum value
238 just before local sunrise (~04:00/05:00 LT), a daytime peak (~13:00/14:00 LT) and then a
239 gradual decrement through the evening and nighttime.
- 240 2. During high solar activity years, measured Ni data exhibited steeper enhancements with a
241 higher magnitude of the peak density as compared to those during the rising and
242 declining phases of solar activity. This shows a direct dependency of the ion density on
243 solar flux.
- 244 3. During all the considered years (1999-2003), IRI-2016 model overestimates Ni data,
245 specifically in the nighttime and pre-sunrise hours. On the contrary, the model
246 underestimates Ni during daytime. Also, the IRI model predicts evening enhancements in
247 Ni which are not observed in ROCSAT-1 measurements.
- 248 4. The annual diurnal analysis of Ti (measured by ROCSAT) shows that Ti exhibits a
249 morning peak (morning overshoot, ~07:00 LT), a daytime trough and a secondary peak
250 (evening enhancement) followed by nighttime minima and a minimum before the sunrise.
- 251 5. According to ROCSAT-1 measurements, secondary peaks of Ti are of higher magnitude
252 (~1500K) for years 2000-2002 as compared to year 1999 and 2003 (~1400K). On the
253 contrary, the IRI-model cannot model the Ti secondary peaks measured by ROCSAT-1.
- 254 6. For each year scatter plots between Ni data measured by ROCSAT-1 and those estimated
255 by the IRI model for years 1999-2003 have been generated; they indicate R^2 value
256 ranging from 0.7-0.8. Analogous scatter plots for Ti show R^2 values ranging from 0.8-
257 0.9.
- 258 7. We have found that Ni and Ti are strongly positively correlated with solar-flux (F10.7).
259 In this case, the correlation coefficient factor R^2 obtained for Ni and Ti during daytime
260 (10:00-16:00 LT) was ~ 0.8 and ~ 0.9 respectively.

261 At last, it can be concluded that an overall evaluation demonstrates a moderate agreement
262 between the IRI-2016 model's estimations and ROCSAT-1 measurements. However, the model
263 still requires some improvements to be done, left as a scope for future work.

264

265 **Acknowledgements**

266 The authors thank NASA CDA Web for making the valuable ROCSAT satellite data available
267 online. Authors acknowledge <https://omniweb.gsfc.nasa.gov/form/dx1.html> and
268 https://ccmc.gsfc.nasa.gov/modelweb/models/iri2016_vitmo.php websites for making the F10.7
269 and IRI data available online. The authors also thank the potential reviewers and the editor for
270 improvising the paper.

271

272

273

274

275

276

277

278

279

280

281

282 **References**

283

284 Aggarwal, M., H. P. Joshi and K. N. Iyer (2007). Solar activity dependence of electron and ion
285 temperatures using SROSS-C2 RPA data and comparison with IRI model, J. Atmos. Solar-Terr.
286 Phys., 69, 860-874.

287 Bailey, G. J., R. J. Moffett, W. B. Hanson and S. Sanatani (1973). Effects of interhemisphere
288 transport on plasma temperatures at low latitudes, J. Geophys. Res., 78, 5597-5610.

289 Bailey, G. J., Y. Z. Su and K. I. Oyama (2000). Yearly variations in the low-latitude topside
290 ionosphere, *Ann. Geophys.*, 18, 789-798.

291 Balan, N., K. I. Oyama, G. J. Bailey, S. Fukao, S. Watanabe and M. A. Abdu (1997). A plasma
292 temperature anomaly in the equatorial topside ionosphere, *J. Geophys. Res.*, 102, 7485-7492.

293 Balan, N., K. I. Oyama, G. J. Bailey and T. Abe (1996). Plasmasphere electron temperature
294 studies using satellite observation and theoretical model, *J. Geophys. Res.*, 101, 15323-15330.

295 Balan, N., Y. Otsuka, S. Fukao, M. A. Abdu and G. J. Bailey (2000). Annual variations of the
296 ionosphere: A review based on MU radar observations, *Adv. Space Research.*, 25, 153-162.

297 Bardhan, A., D. K. Sharma and J. Rai (2014). Variation of O⁺ ion density during low and high
298 solar activity as measured by SROSS-C2 satellite, *Atmosfera*, 27(3), 227-237.

299 Bardhan, A., D. K. Sharma, M. S. Khurana, M. Aggarwal and S. Kumar (2015). Electron -ion-
300 neutral temperatures and their ratio comparisons over low latitude ionosphere, *Adv. Space Res.*,
301 56, 2117-2129.

302 Bhuyan, P. K. and P. K. Kakoty (2001). A modeling study of Indian low latitude ionosphere:
303 Part I I- Results and comparison with SROSS-C2 satellite data, *Ind. J. Radio. Space Phys.*, 30,
304 66-71

305 Bhuyan, P. K., P. K. Kakoty and S.B. Singh (2002). Theoretical simulation of O⁺ and H⁺
306 densities in the Indian low latitude F-region and comparison with observations, *Ann. Geophys.*,
307 European Geosciences Union, 20(12), 1959-1966.

308 Bilitza, D. (1991). Electron and ion temperature data for ionosphere modeling, *Adv. Space Res.*,
309 11: 10(139)- (10)148.

310 Bilitza, D. (2000). International reference ionosphere, *Radio Science*, 36, 261-275.

311 Bilitza, D., D. Altadill, V. Truhlik, V. Shubin, I. Galkin, B. Reinisch and X. Huang (2017).
312 International reference ionosphere 2016: From ionospheric climate to real-time weather
313 predictions, *Space Weather*, 15, 418-429.

314 Borgohain, A. and P. K. Bhuyan (2012). Effect of solar cycle on topside ion temperature
315 measured by SROSS-C2 and ROCSAT-1 over the Indian equatorial and low latitudes, *Ann.*
316 *Geophys.*, 30, 1645- 1654, doi:10.5194/angeo-30-1645-2012.

317 Chang, Y. S., W. L. Chiang, S. J. Ying, B. J. Holt, C. R. Lippincott and K. C. Hsieh (1999).
318 System architecture of the IPEI payload on ROCSAT-1, *Terr. Atmos. Oceanic Sci.*, 10(IS3),
319 suppl., 7-18.

320 Farley, F.T., J. P. McClure, D. L. Sterling and J. L. Green (1967). Temperature and Composition
321 of the Equatorial Ionosphere, *J. Geophys. Res.*, 72, 5837-5851.

322 Fejer, B. G. (1997). The electrodynamics of the low-latitude ionosphere: Recent results and
323 future challenges, *J. Atmos. Solar Terr. Phys.*, 59, 1456-1482.

324 Hanson, W. B. and R. J. Moffett (1966). Ionization transport effects in the equatorial F-region. *J.*
325 *Geophys. Res.*, 71, 5559-5572.

326 Hanson, W. B., A. F. Nagy and R.J. Moffett (1973). Measurements of supercooled plasma in the
327 equatorial exosphere, *J. Geophys. Res.*, 78, 751-756.

328 Liu, L., B. Zhao, W. Wan, S. Venkatraman, M. L. Zhang and X. Yue (2007a). Yearly variations
329 of global plasma densities in the topside ionosphere at middle and low latitudes, *J. Geophys. Res.*,
330 112, A07303, doi:10.1029/2007JA012283.

331 Liu, L., W. Wan, X. Yue, B. Zhao, B. Ning and M.-L. Zhang (2007b). The dependence of plasma
332 density in the topside ionosphere on solar activity level, *Ann. Geophys.*, 25(6), 1337-1343.

333 Martyn, D. F. (1947). Atmospheric tides in ionosphere. I. Solar tides in F2-region. *P. Roy. Soc.*
334 *Lond. A Mat.* 189, 241-260.

335 Mendillo, M., C. Huang, X. Pi, H. Rishbeth and R. Meier (2005). The global ionospheric
336 asymmetry in total electron content, *J. Atmos. Solar Terr. Phys.*, 67, 1377-1387.

337 Otsuka, Y., S. Kawamura, N. Balan, S. Fukao and G. J. Bailey (1998). Temperature variations in
338 the ionosphere over the MU radar, *J. Geophys. Res.*, 103, 20, 705.

339 Oyama, K. I., S. Watanabe, Y. Su, T. Takahashi and K. Hirao (1996). Season, local time and
340 longitude variations of electron temperature at the height of 600km in the low-latitude region,
341 *Adv. Space Res.*, 18, 269-278.

342 Prabhakaran Nayar, S. R., L.T. Alexander, V. N. Radhika, T. John, P. Subramanyam, P. Chopra,
343 M. Bahl, H. K. Maini, V. Maini, V. Singh, D. Singh and S. C. Garg (2004). Observation of
344 periodic fluctuations in electron and ion temperature at the low latitude upper ionosphere by
345 SROSS-C2 satellite, *Ann. Geophys.*, 22, 1665-1674, doi:10.5194/angeo-22-1665-2004.

346 Ren, Z., W. Wan, L. Liu, B. Zhao, Y. Wei, X. Yue and R. A. Heelis (2008). Longitudinal
347 variations of electron temperature and total ion density in the sunset equatorial topside
348 ionosphere, *Geophys. Res. Lett.*, 35, L05108, doi:10.1029/2007GL03299

349 Rishbeth, H. and I. C. F. Muller-Wodarg (2006). Why is there more ionosphere in January than in
350 July? The annual asymmetry in the F2-Layer, *Ann. Geophys.*, 24, 3293-3311.

351 Sharma, P. K., P. P. Pathak, D. K. Sharma, J. Rai (2010). Variation of ionospheric electron and
352 ion temperatures during periods of minimum to maximum solar activity by the SROSS-C2
353 satellite over Indian low and equatorial latitudes, *J. Adv. Space Res.*, 45, 294-302.

354 Su, S. Y., H. C. Yeh, R. A. Heelis, J. M. Wu, S. C. Yang, L. F. Lee and H. L. Chen (1999). The
355 ROCSAT-1 IPEI preliminary results: Low-latitude plasma and flow variations, *Terr. Atmos.*
356 *Oceanic Sci.*, 10, 787-804.

357 Su, Y. Z., G. J. Bailey and K. I. Oyama (1998). Annual and seasonal variations in the low
358 latitude topside ionosphere, *Ann. Geophys.*, 16, 974-985, doi:10.1007/s00585-998-0974-0.

359 Su, Y. Z., K.-I. Oyama, G. J. Bailey, T. Takahashi and S. Watanabe (1995). Comparison of
360 satellite electron density and temperature measurements at low latitudes with a plasmasphere-
361 ionosphere model, *J. Geophys. Res.*, 100, 14591-14604.

362 Tapping, K. F. (2013). The 10.7cm solar radio flux (F10.7), *Space Weather*, 11, 394-406,
363 doi:10.1002/swe.20064.

364 Watanabe, S. and K. I. Oyama (1996). Effects of neutral wind on the electron temperature at the
365 height of 600 km in the low latitude region, *Annales Geophysicae*, 14(3), 290-296,
366 doi:10.1007/s00585-996-0290-5.

367 Yeh, H. C., S. Y. Su, Y. C. Yeh, J. M. Wu, R. A. Heelis and B. J. Holt (1999a). Scientific
368 mission of the IPEI payload onboard ROCSAT-1, *J. Terr. Atmos. Oceanic Sci.*, suppl., 19-42.

369 Yeh, H. C., S.-Y. Su, R. A. Heelis and J. M. Wu (1999b). The ROCSAT-1 IPEI preliminary
370 results: Vertical iondrift statistics, *J. Terr. Atmos. Oceanic Sci.*, 10, 805-820.

371 Zhang, S. R. and J. M. Holt (2004). Ionospheric plasma temperatures during 1976-2001 over
372 Millstone Hill, *J. Adv. Space Res.*, 33, 963-969.

373 Zou, L., H. Rishbeth, I. C. F. Muller-Wodarg, A. D. Aylward, G. H. Millward, T. J. Fuller-
374 Rowell, D. W. Idenden and R. J. Moffett (2000). Annual and semiannual variations in the
375 ionospheric F2-layer, I. Modelling, *Ann. Geophys.*, 18, 927.

376

377

378

379

380

381
382
383
384
385
386
387
388
389
390
391
392
393
394
395
396
397
398
399
400
401
402
403
404
405

Figure captions

Figure 1: Variation of Solar Flux (F10.7, sfu) (upper panel) and yearly averaged data count as measured by ROCSAT-1 satellite (lower panel), for years 1999-2003.

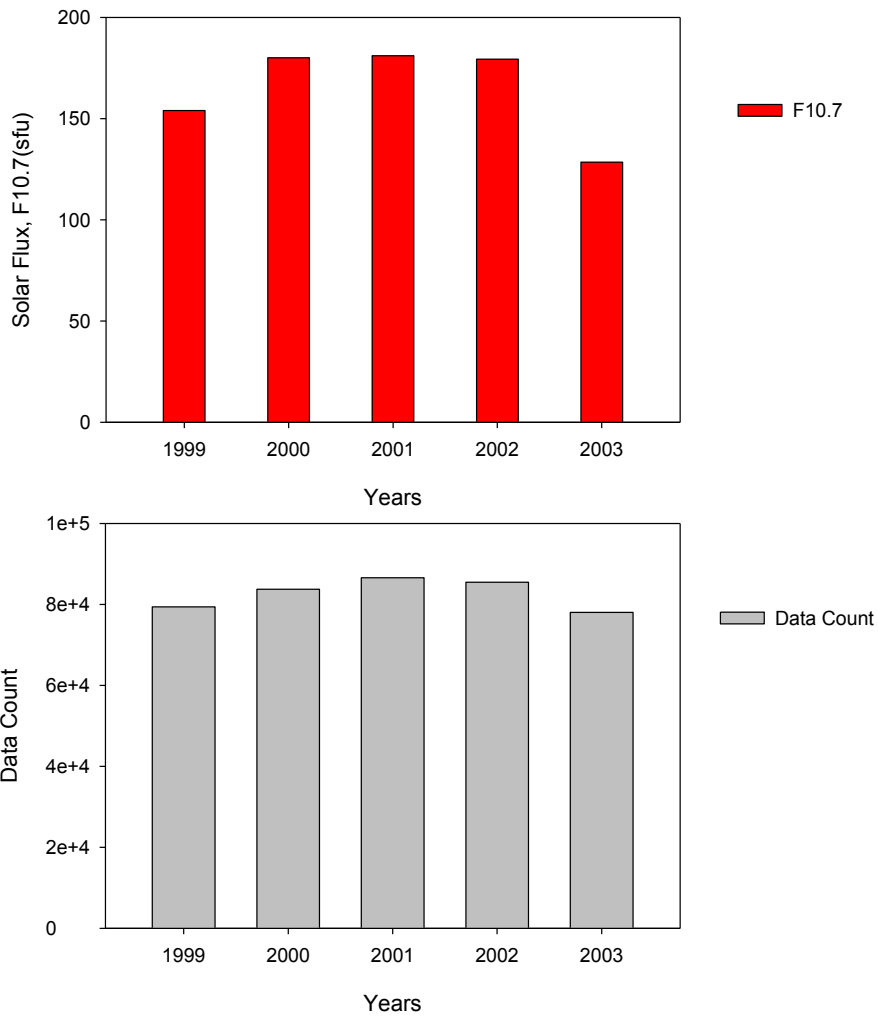
Figure 2: Annual variation of Ni (cm^{-3}) measured by ROCSAT-1 (red color) and estimated by IRI-2016 model (black color) for years 1999-2003.

Figure 3: Annual variation of Ti (K) measured by ROCSAT-1 (red color) and estimated by IRI-2016 (black color) for years 1999-2003.

Figure 4: Variation of Ni measured by ROCSAT-1 relative to Ni estimated by IRI-2016 on a diurnal scale for years 1999-2003 (upper panels). Scatter plots of two data sets, along with the corresponding linear fits and correlation coefficient values obtained for hourly averaged daytime values (10-16 LT) of Ni (lower panels).

Figure 5: Variation of Ti measured by ROCSAT-1 relative to Ti estimated by IRI-2016 on a diurnal scale for years 1999-2003 (upper panels). Scatter plots of two data sets, along with the corresponding linear fits and correlation coefficient values obtained for hourly averaged daytime values (10-16 LT) of Ti (lower panels).

Figure 6: Scatter plots between yearly averaged values of (left panels) Ni, cm^{-3} and solar flux F10.7, sfu, and between averaged values of (right panels) Ti (K) and solar flux F10.7, sfu, for (upper panels) ROCSAT-1 and (lower panels) IRI-2016, for years 1999-2003.



406

Figure 1: Variation of Solar Flux (F10.7, sfu) (upper panel) and yearly averaged data count as measured by ROCSAT-1 satellite (lower panel), between years 1999-2003.

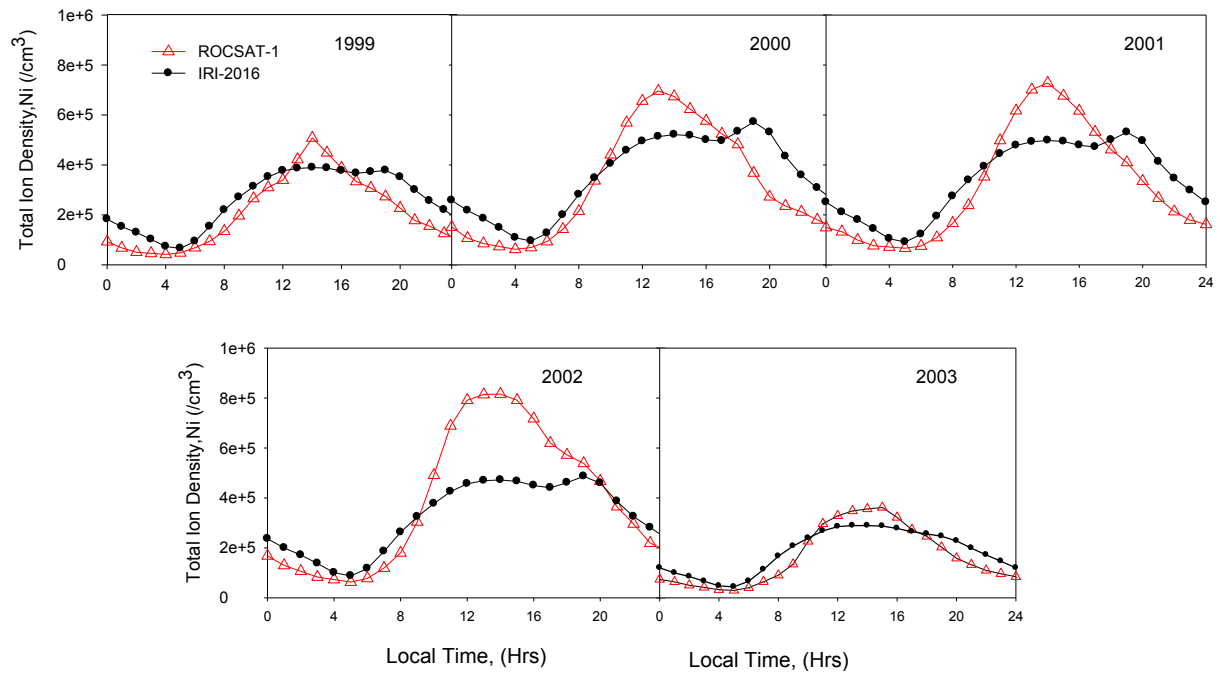
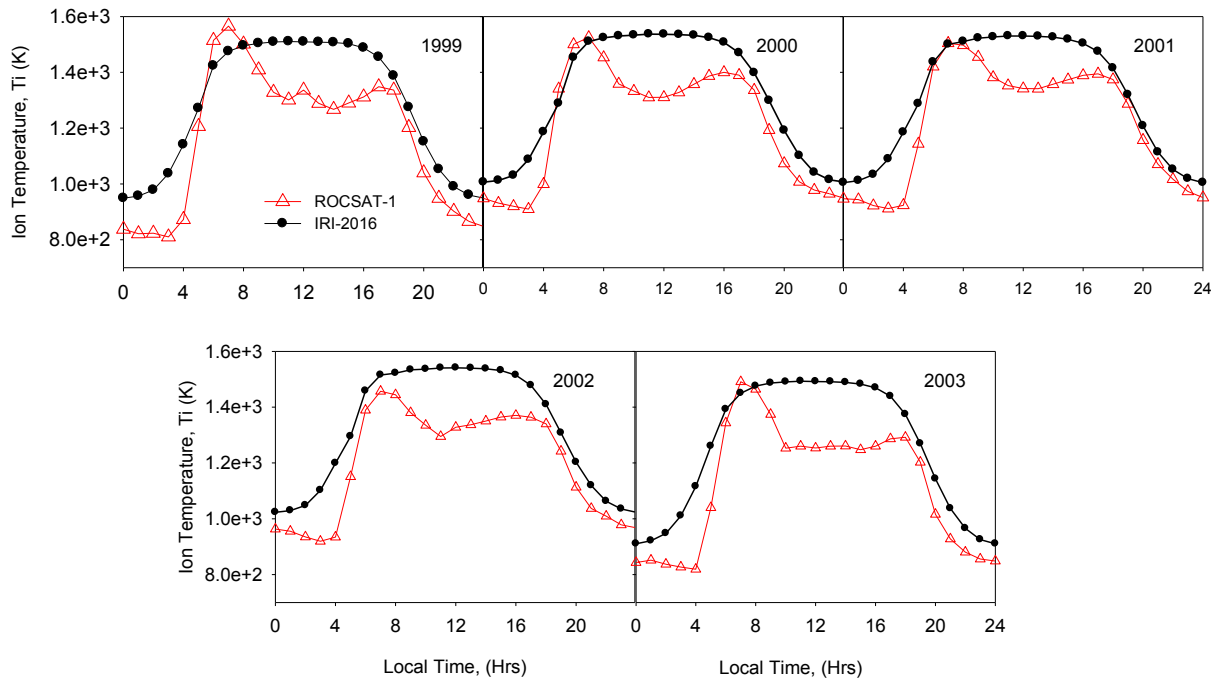


Figure 2: Annual variation of Ni (cm^{-3}) measured by ROCSAT-1 (red color) and estimated by IRI-2016 model (black color) for years 1999-2003.

407
 408
 409
 410
 411
 412
 413
 414
 415
 416
 417
 418
 419
 420
 421
 422



424

425

Figure 3: Annual variation of Ti (K) measured by ROCSAT-1 (red color) and estimated by IRI-2016 (black color) for years 1999-2003.

426

427

428

429

430

431

432

433

434

435

436

437

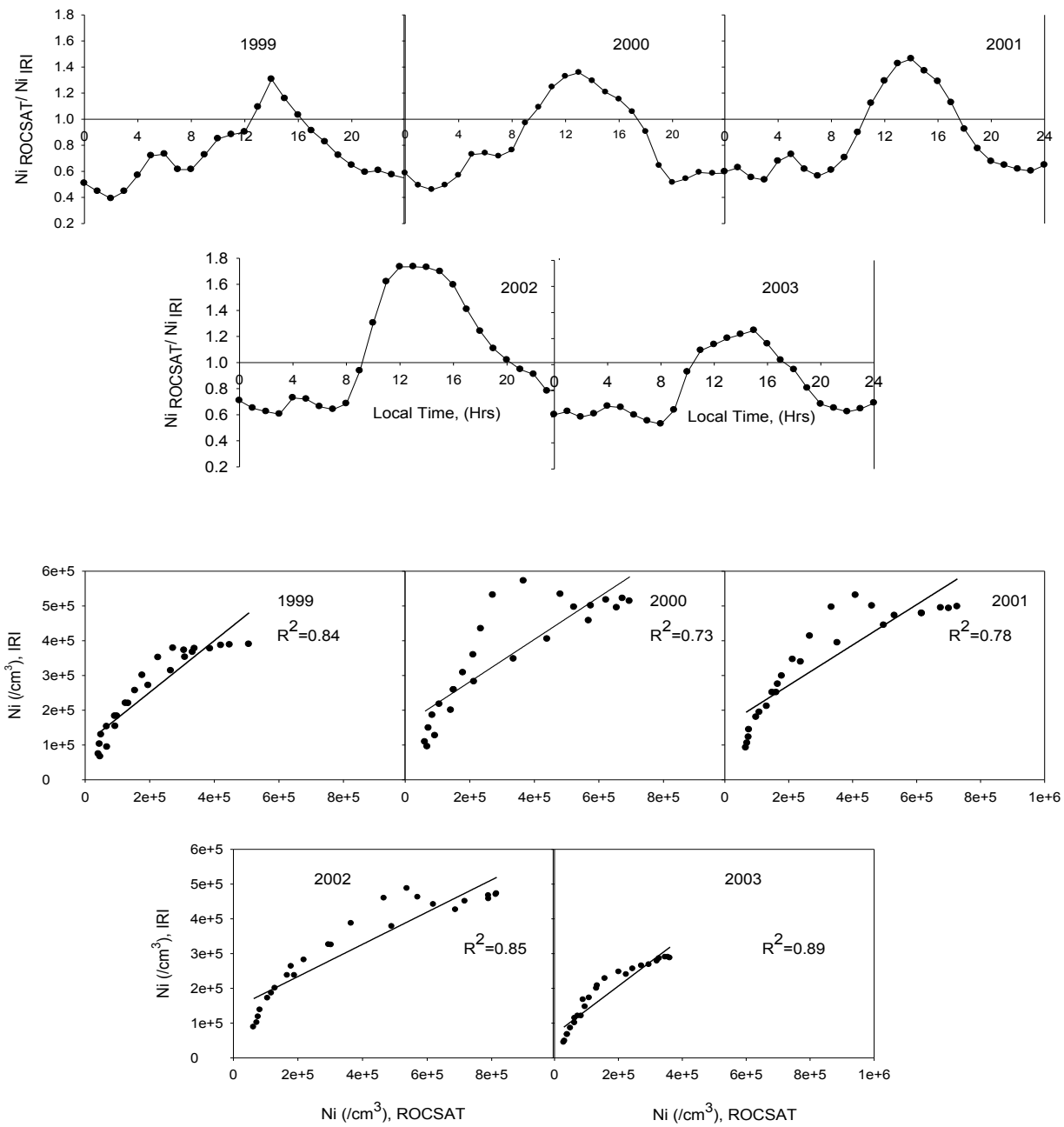
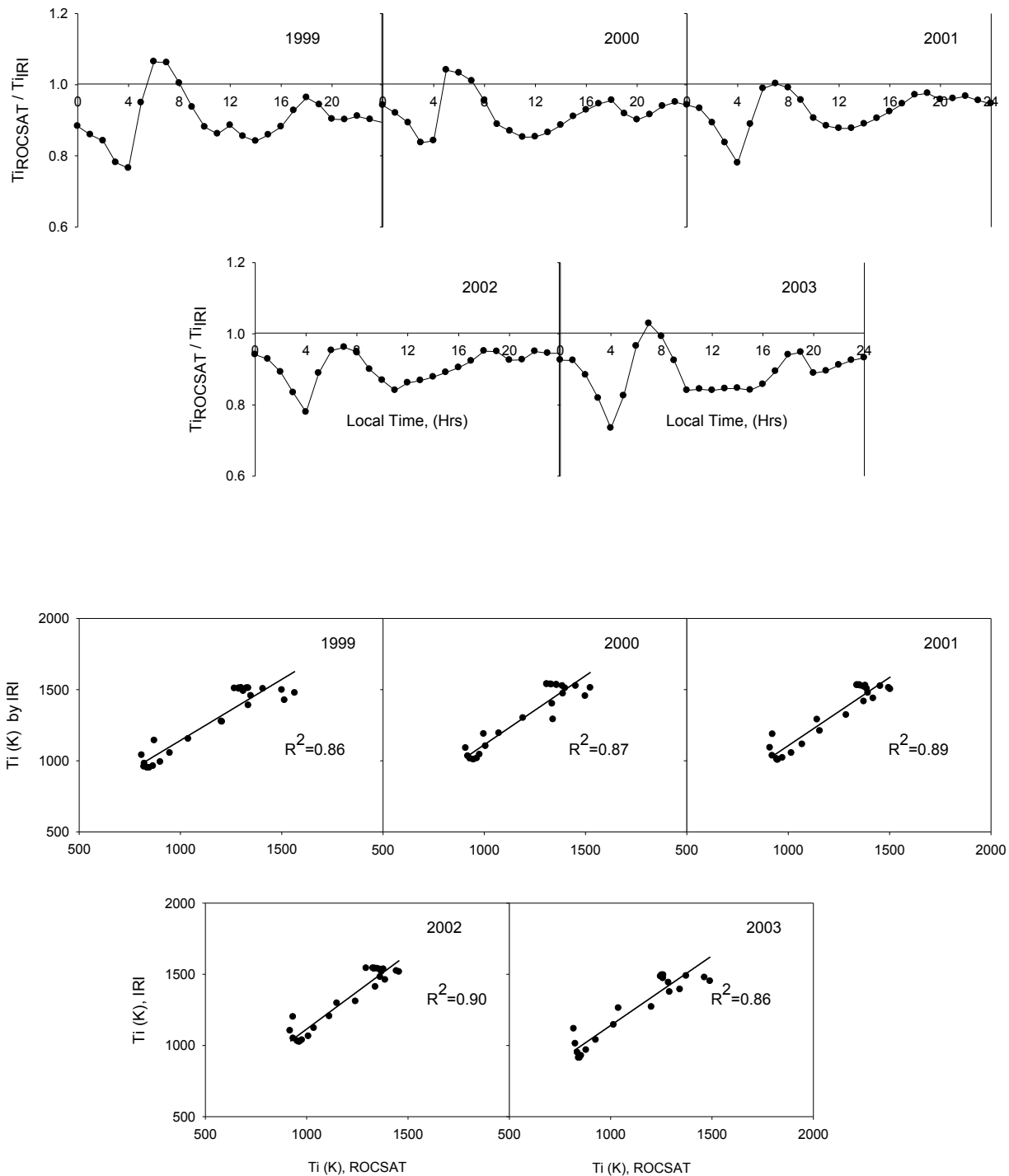


Figure 4: Variation of Ni measured by ROCSAT-1 relative to Ni estimated by IRI-2016 on a diurnal scale for years 1999-2003(upper panels). Scatter plots of two data sets, along with the corresponding linear fits and correlation coefficient values obtained for hourly averaged daytime values (10-16 LT) of Ni (lower panels).

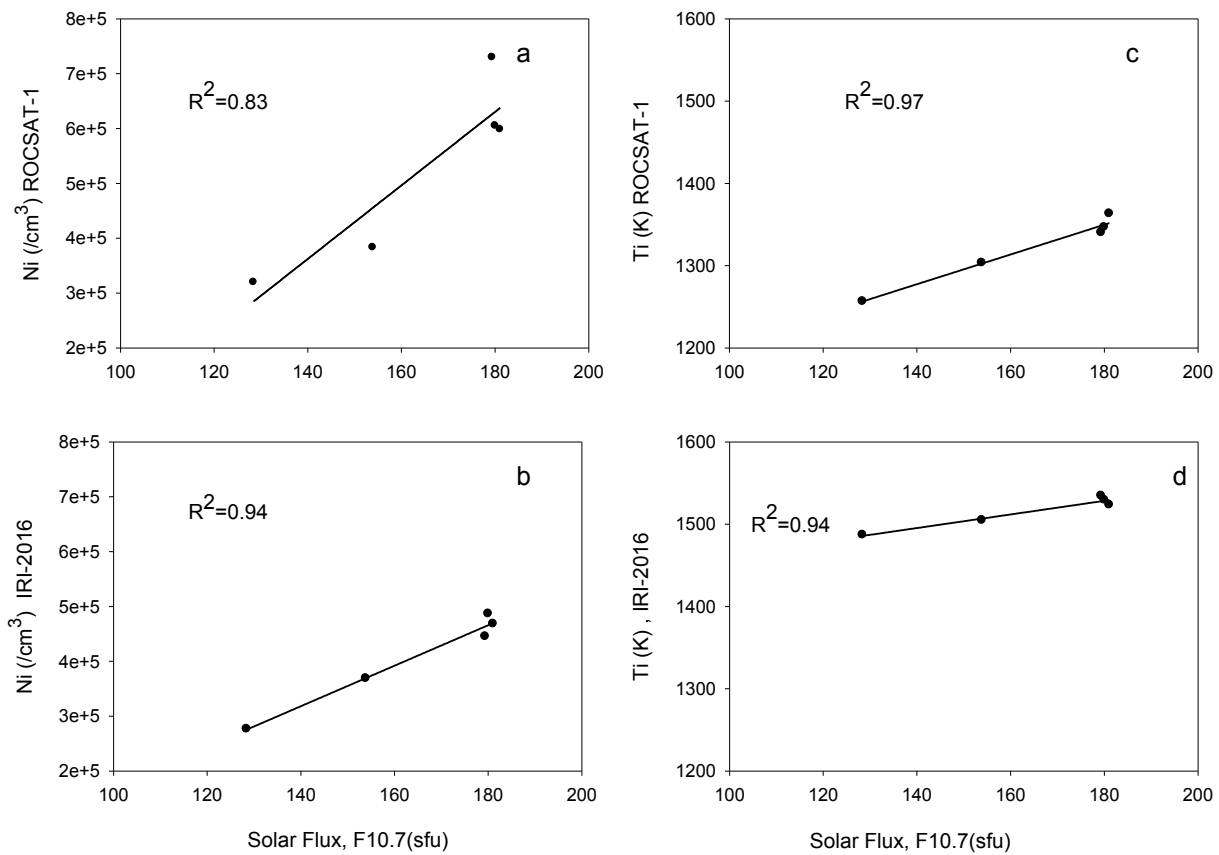


441

442

443

Figure 5: Variation of Ti measured by ROCSAT-1 relative to Ti estimated by IRI-2016 on a diurnal scale for years 1999-2003 (upper panels). Scatter plots of two data sets, along with the corresponding linear fits and correlation coefficient values obtained for hourly averaged daytime values (10-16 LT) of Ti (lower panels).



444

445

446

447

448

449

450

451

452

453

454

Figure 6: Scatter plots between yearly averaged values of (left panels) Ni, cm^{-3} and solar flux F10.7, sfu, and between averaged values of (right panels) Ti (K) and solar flux F10.7, sfu, for (upper panels) ROCSAT-1 and (lower panels) IRI-2016, for years 1999-2003.